

RSC Applied Interfaces

Accepted Manuscript

This article can be cited before page numbers have been issued, to do this please use: D. Dang, Y. Pham, D. Zhou, D. Le, M. Terrones, M. Phan and L. Woods, *RSC Appl. Interfaces*, 2025, DOI: 10.1039/D5LF00113G.







This is an Accepted Manuscript, which has been through the Royal Society of Chemistry peer review process and has been accepted for publication.

Accepted Manuscripts are published online shortly after acceptance, before technical editing, formatting and proof reading. Using this free service, authors can make their results available to the community, in citable form, before we publish the edited article. We will replace this Accepted Manuscript with the edited and formatted Advance Article as soon as it is available.

You can find more information about Accepted Manuscripts in the [Information for Authors](#).

Please note that technical editing may introduce minor changes to the text and/or graphics, which may alter content. The journal's standard [Terms & Conditions](#) and the [Ethical guidelines](#) still apply. In no event shall the Royal Society of Chemistry be held responsible for any errors or omissions in this Accepted Manuscript or any consequences arising from the use of any information it contains.

Interface Magnetism in Vanadium-doped MoS₂/Graphene Heterostructures

Diem Thi-Xuan Dang [†], Yen Thi-Hai Pham,^{†,§} Da Zhou,^{‡,¶} Dai-Nam Le [†],
Mauricio Terrones,^{‡,¶} Manh-Huong Phan ^{*,†} and Lilia M. Woods ^{*,†}

[†]*Department of Physics, University of South Florida, Tampa, Florida 33620, USA*

[‡]*Department of Physics, The Pennsylvania State University, University Park,
Pennsylvania 16802, USA*

[¶]*Center for 2- Dimensional and Layered Materials, The Pennsylvania State University,
University Park, Pennsylvania 16802, USA*

[§]*Current address: Department of Physics and Astronomy, George Mason University,
Fairfax, Virginia 22030, USA*

E-mail: phanm@usf.edu; lmwoods@usf.edu

Abstract

Magnetism in two-dimensional materials is of great importance in discovering new physical phenomena and developing new devices at the nanoscale. In this paper, first-principles simulations are used to calculate the electronic and magnetic properties of heterostructures composed of Graphene and MoS₂ considering the influence of point defects and Vanadium doping. It is found that the concentration of the dopants and the types of defects can result in induced magnetic moments leading to ferromagnetically polarized systems with sharp interfaces. This provides a framework for interpreting the experimental observations of enhanced ferromagnetism in both MoS₂/Graphene and V-doped MoS₂/Graphene heterostructures. The computed electronic and spin polarizations give a microscopic understanding of the origin of ferromagnetism in these systems



and illustrate how doping and defect engineering can lead to targeted property tunability. Our work has demonstrated that through defects engineering, ferromagnetism can be achieved in V-doped MoS₂/Graphene heterostructures, providing a potential way to induce magnetization in other TMDC/Graphene materials and opening new opportunities for their applications in nano-spintronics.

1 Introduction

The properties of low-dimensional materials and heterostructures (HSTs), in which relatively weak dispersion interactions play an important role, are strongly modified by the proximity effect. A prominent example is Graphene, which experiences relatively strong proximity spin-orbit coupling (SOC) effects when placed on transition metal dichalcogenides (TMDC). Low-dimensional HSTs are currently used in optospintronics,^{1,2} as well as in a variety of applications where the spin Hall effect and the spin galvanic effect are prominent.^{3,4}

Typically, TMDC/Graphene HSTs are non-magnetic. Nevertheless, the development of methods to effectively generate and control magnetism in 2D materials is critical for the establishment of new magnetic HSTs with various applications. An effective method to induce magnetic properties in 2D semiconductors involves doping and defect engineering.^{5,6} Based on previous studies, transition metal substitutional doping can effectively generate tunable magnetism in TMDC systems.^{7,8} Among them, Vanadium doping can realize not only p-type transport behavior in TMDCs but also room-temperature ferromagnetism, making V-doped TMDCs a favorable platform for electronic and spintronic devices.^{9,10}

Recently, V-doped MoS₂ has been intensively studied. Zhang et al. demonstrated that V-doped MoS₂ increases radiative recombination of excitons relative to trions by reducing background electrons in MoS₂.¹¹ Sahoo et al. reported the presence of time-reversal asymmetry between the two K-valleys with a 32 meV relative energy shift between them.¹² Maity et al. observed a semiconductor-to-metal transition in V-doped MoS₂ alloy when the doping concentration increased above 5%.¹³ The magnetic performance of the V-doped MoS₂ can be



tuned by varying the doping concentration. In particular, enhanced ferromagnetism is observed for up to 3% V doping concentration,¹⁴ which is strongly inhibited by raising doping beyond 8%.¹⁴ However, due to the low doping concentration, the net magnetization of these monolayers remains relatively weak limiting their suitability for spintronic and magnetic sensor applications.

Constructing a HST of a doped TMDC exhibiting ferromagnetic behavior and a non-magnetic 2D system such as Graphene brings forward new possibilities for magnetic HSTs with sharp interfaces. Of special interest is to see if Graphene can become magnetic as a result of interactions and proximity effects with the ferromagnetic TMDC.^{15,16} In this study, we broaden our understanding of doped TMDCs and their magnetism by investigating V-doped MoS₂/Graphene HSTs by taking into account various types of defects and doping concentrations. In Graphene, mono- and divacancies, Stone-Wales defects, etc. have been studied quite extensively.^{17,18} The fabrication of TMDCs can also result in various types of vacancies,^{19,20} including V-doped MoS₂ monolayer obtained by chemical vapor deposition methods.¹⁴ These vacancies are known to have dramatic effects on the electronic, magnetic, and optical properties of TMDC systems.^{14,21,22} Due to their importance, in this paper, we have systematically studied the role of point defects in the properties of the V-doped MoS₂/Graphene HST. We present various types of defect formations, the electronic structures of the defective materials, and the defect signatures of the magnetic properties of the different HSTs. Our work shows pathways to improve the saturation magnetization of TMDC/Graphene HSTs, which can be useful for their application in spintronics.

2 Results and Discussions

2.1 Structural properties

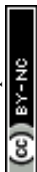
The primary investigation system is an HST formed by stacking a single Graphene layer (Gr) and a single MoS₂ layer. To initiate the calculations, we construct an atomistic supercell



consisting of 162 C atoms ($9 \times 9 \times 1$ Gr unit cell) and 49 Mo, 98 S atoms ($7 \times 7 \times 1$ MoS₂ unit cell). After relaxation, the in-plane lattice constant of the Gr/MoS₂ HST is $a = b = 22.183$ Å. As a reference, each monolayer is also simulated separately with an optimized lattice constant for Gr found as $a = b = 2.471$ Å, while the optimized lattice constant for MoS₂ is $a = b = 3.153$ Å.

In addition to a HST composed of pristine monolayers, several point-like defects in both monolayers are considered, because isolated point defects are unavoidable in the synthesis process as discussed earlier. Specifically, a C monovacancy (Gr+V_C), C divacancies (Gr+V_{2C}) and Stone-Wales (Gr+V_{SW}) defect are constructed in the Gr part of the supercell. The defective TMDC monolayers are also generated in the MoS₂ part of the supercell and they are: MoS₂+V_S (with a S monovacancy), MoS₂+V_{S-S} (with two adjacent S vacancies on the same S layer), MoS₂+V_{2S} (with two S vacancies on the same Mo atom but in opposite S layers), MoS₂+V_{Mo} (with a Mo monovacancy) and MoS₂+V_{Mo+2S} (with a Mo vacancy and two S vacancies on opposite layers). To probe the magnetism in the system, Vanadium substitutional dopants at the Mo sites in the TMDC layer are simulated by taking V_{0.02}Mo_{0.98}S₂ (2% V doping) and V_{0.04}Mo_{0.96}S₂ (4% V doping) monolayers. Various combinations for the combined effect of point defects and dopants within the MoS₂ layer are also taken by constructing V_{0.02}Mo_{0.98}S₂+V_S (2% V doping and a S monovacancy), V_{0.02}Mo_{0.98}S₂+V_{S-S} (2% V doping and two adjacent S vacancies on the same layer), V_{0.02}Mo_{0.98}S₂+V_{2S} (2% V doping and two adjacent S vacancies on the different layer), V_{0.02}Mo_{0.98}S₂+V_{Mo} (2% V doping and a Mo monovacancy), and V_{0.02}Mo_{0.98}S₂+V_{Mo+2S} (with 2% V doping, a Mo vacancy and two adjacent S vacancies on the different layers) monolayers.

In this study, we simulate HSTs composed of various combinations of Gr and TMDC sheets discussed above. We find that the magnetic properties of HSTs composed of different TMDCs and pristine Gr or Gr+V_{2C} or Gr+V_{SW} are very similar due to the similar nonmagnetic nature of these Gr sheets. Thus, in what follows, we only consider HSTs composed of different TMDCs and pristine Gr or Gr+V_C. The full list of the simulated HSTs composed



of various combinations of defective and/or doped monolayers is given in Table 1, and several representative examples of the lattice configurations are shown in Fig. 1. The numerous combinations (26 structures altogether) help us to understand the complex interplay between the types of point defects in a specific monolayer and the magnetic dopants in the Gr/MoS₂ HSTs.

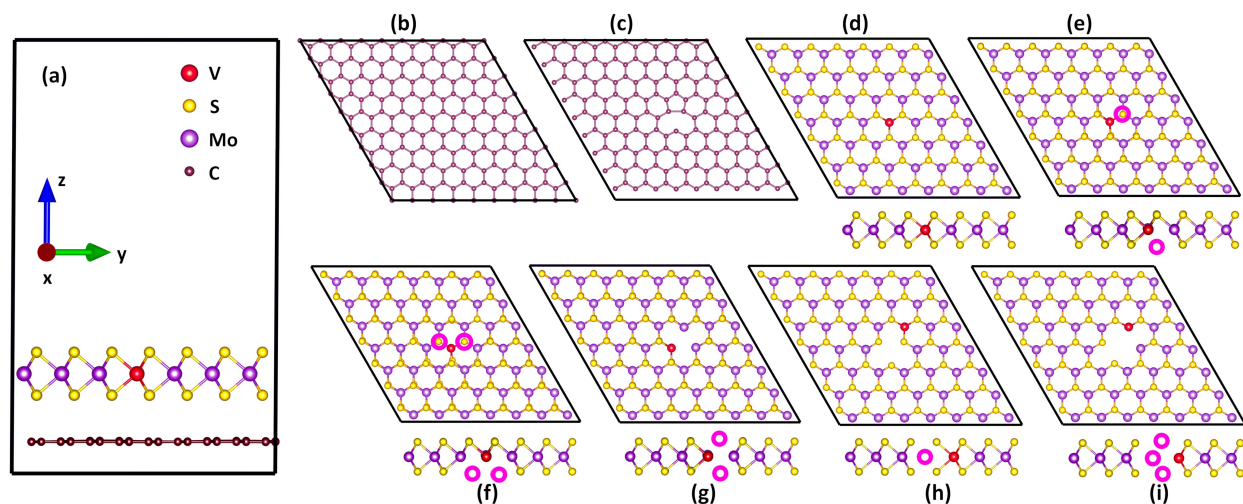


Figure 1: (a) Side view of the pristine HST showing labels for the different atoms and the interlayer separation d . Top views of the Gr monolayers as part of the V-doped MoS₂/Gr HSTs: (b) pristine Gr, (c) Gr+V_C (with C monovacancy). Top and side views of the various V_{0.02}Mo_{0.98}S₂ monolayers as part of the V-doped MoS₂/Gr HSTs: (d) V_{0.02}Mo_{0.98}S₂ (with 2% V substitutional doping), (e) V_{0.02}Mo_{0.98}S₂+V_S (with 2% V substitutional doping and S monovacancy), (f) V_{0.02}Mo_{0.98}S₂+V_{S-S} (with 2% V doping and S divacancies on the same atomic layer), (g) V_{0.02}Mo_{0.98}S₂+V_{2S} (with 2% V substitutional doping and S divacancies on different atomic layers), (h) V_{0.02}Mo_{0.98}S₂+V_{Mo} (with 2% substitutional V doping and Mo monovacancy), (i) V_{0.02}Mo_{0.98}S₂+V_{Mo+2S} (with 2% V doping and an Mo+2S defect complex).

Table 1 shows the lattice mismatch of each HST by giving the strain each layer experiences in the supercell after full relaxation. It appears that upon the formation of the different HSTs, the Gr layer is shrunk while the TMDC layer is expanded, but in all cases the effect is less than a percent. For example, V_{0.02}Mo_{0.98}S₂ sheet in Gr/V_{0.02}Mo_{0.98}S₂ HST is stretched by 0.426%, whereas the Gr sheet is compressed by 0.247% from the optimized pristine cell parameters. V_{0.02}Mo_{0.98}S₂ sheet in (Gr+V_C)/V_{0.02}Mo_{0.98}S₂ HST is stretched by 0.462%, while the Gr sheet is compressed by 0.234% from the optimized parameters of the pristine cell.



These rather small values for the built-in stress (less than 1 % overall) do not change the properties of the monolayers and their HSTs, in agreement with other similar systems.²³

Table 1: Built-in strain in each monolayer calculated using $\epsilon = \frac{a_{HST} - a_i}{a_i} \times 100\%$ (a_{HST} - lattice constant of the HST; a_i - lattice constant of the Gr or TMDC layers)

Name	Gr Strain (%)	TMDC Strain (%)	Name	Gr+V _C Strain (%)	TMDC Strain (%)
HST1: Gr/MoS ₂	-0.234	0.498	HST14: (Gr+V _C)/MoS ₂	-0.225	0.530
HST2: Gr/(MoS ₂ +V _S)	-0.283	0.644	HST15: (Gr+V _C)/(MoS ₂ +V _S)	-0.288	0.654
HST3: Gr/(MoS ₂ +V _{S-S})	-0.337	0.824	HST16: (Gr+V _C)/(MoS ₂ +V _{S-S})	-0.351	0.833
HST4: Gr/(MoS ₂ +V _{2S})	-0.342	0.778	HST17: (Gr+V _C)/(MoS ₂ +V _{2S})	-0.342	0.782
HST5: Gr/(MoS ₂ +V _{Mo})	-0.220	0.489	HST18: (Gr+V _C)/(MoS ₂ +V _{Mo})	-0.197	0.534
HST6: Gr/(MoS ₂ +V _{Mo+2S})	-0.382	0.806	HST19: (Gr+V _C)/(MoS ₂ +V _{Mo+2S})	-0.697	0.708
HST7: Gr/V _{0.02} Mo _{0.98} S ₂	-0.247	0.426	HST20: (Gr+V _C)/V _{0.02} Mo _{0.98} S ₂	-0.234	0.462
HST8: Gr/V _{0.04} Mo _{0.96} S ₂	-0.229	0.389	HST21: (Gr+V _C)/V _{0.04} Mo _{0.96} S ₂	-0.499	0.407
HST9: Gr/(V _{0.02} Mo _{0.98} S ₂ +V _S)	-0.288	0.535	HST22: (Gr+V _C)/(V _{0.02} Mo _{0.98} S ₂ +V _S)	-0.306	0.512
HST10: Gr/(V _{0.02} Mo _{0.98} S ₂ +V _{S-S})	-0.351	0.723	HST23: (Gr+V _C)/(V _{0.02} Mo _{0.98} S ₂ +V _{S-S})	-0.373	0.723
HST11: Gr/(V _{0.02} Mo _{0.98} S ₂ +V _{2S})	-0.346	0.714	HST24: (Gr+V _C)/(V _{0.02} Mo _{0.98} S ₂ +V _{2S})	-0.364	0.695
HST12: Gr/(V _{0.02} Mo _{0.98} S ₂ +V _{Mo})	-0.234	0.631	HST25: (Gr+V _C)/(V _{0.02} Mo _{0.98} S ₂ +V _{Mo})	-0.184	0.480
HST13: Gr/(V _{0.02} Mo _{0.98} S ₂ +V _{Mo+2S})	-0.292	0.800	HST26: (Gr+V _C)/(V _{0.02} Mo _{0.98} S ₂ +V _{Mo+2S})	-0.306	0.809

To gain some insight into the interface properties of the HSTs, we compute the interlayer binding energy using the relation $E_b = (E_{HST} - E_{L1} - E_{L2})/N$, where E_{HST} is the total energy of each HST, $E_{L1,L2}$ are the total energies for the individual monolayers, and N is the number of atoms in the system. Fig. 2 displays E_b versus the interlayer separation d for all systems. The results show that the binding energy is in the range $E_b = (-30.152, -26.772)$ meV/atom, while the interlayer separation varies in $d = (2.885, 3.334)$ Å range. The stability of all HSTs is reflected in the negative values of E_b , and we find that those systems containing MoS₂ with a S monovacancy or divacancies have the highest binding energy. On the other hand, the lowest binding energy is found for systems containing MoS₂ with a Mo+2S vacancy complex or V dopants, indicating that such HSTs have a better structural stability compared to the rest of the systems. These E_b values are typical for HSTs in which van der Waals (vdW) interactions play an important role in their structural stability.²⁴

The interlayer separation in all cases is also in the typical vdW range, since for all systems d is found to be greater than the sum of the covalent radii of C and S atoms (0.76 and 1.05 Å, respectively). For Gr/V_{0.04}Mo_{0.96}S₂ HST, d is very similar to the case of the pristine Gr/V_{0.02}Mo_{0.98}S₂ HST. However, it appears that d between Gr and defective V_{0.02}Mo_{0.98}S₂ monolayers is smaller as compared to the one for the pristine Gr/V_{0.02}Mo_{0.98}S₂ HST. This



effect becomes more pronounced for the defective Gr.

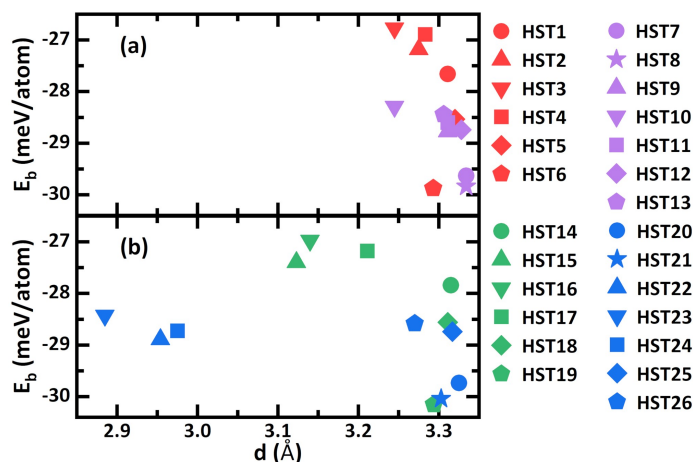


Figure 2: Interlayer binding energy E_b (eV) as a function of the interlayer separation d (Å) of HSTs: (a) Gr/TMDCs and (b) (Gr+V_C)/TMDCs.

2.2 Magnetic properties

The interplay between defects and dopants also affects the magnetic properties of the studied HSTs. Our calculations show that several materials exhibit a ferromagnetic ordering, and in Fig. 3 we show results for the total magnetic moment of the system M_{tot} , and the total magnetic moment for the corresponding Gr layer, M_{Gr} , and TMDC layer, M_{TMDC} .

Let us first examine the isolated MoS₂ monolayer. From the calculations, we find that isolated S monovacancy and divacancies, and Mo monovacancy do not induce magnetic ordering in the isolated TMDC monolayer. This agrees with previous studies on defective and single-doped MoS₂.²⁵ The total magnetic moment is $2 \mu_B$ for MoS₂+V_{Mo+2S}. On the other hand, $M_{tot} = 1 \mu_B$ for a V-doped MoS₂ with or without S monovacancy, S divacancies, Mo monovacancy (V_{0.02}Mo_{0.98}S₂, V_{0.02}Mo_{0.98}S₂+V_S, V_{0.02}Mo_{0.98}S₂+V_{S-S}, V_{0.02}Mo_{0.98}S₂+V_{2S}, V_{0.02}Mo_{0.98}S₂+V_{Mo}). Increasing of the doping concentration raises M_{tot} to $2 \mu_B$ for V_{0.04}Mo_{0.96}S₂, while $M_{tot} = 3 \mu_B$ for V_{0.02}Mo_{0.98}S₂+V_{Mo+2S}. Such synergistic effects have been observed experimentally.²⁶

This situation changes upon the HST formation by adding a Gr layer. In fact, Fig. 3



shows that there is a tendency of reducing the total magnetization when a pristine Gr is stacked above a MoS₂ with mono or divacancies despite their V dopants. It is interesting to observe that $M_{tot} = 1 \mu_B$ of the stand-alone V_{0.02}Mo_{0.98}S₂ becomes $M_{tot} = 0$ for Gr/V_{0.02}Mo_{0.98}S₂. In other words, a ferromagnetic standalone MoS₂ with a 2% V doping becomes nonmagnetic upon bringing Gr together (HST7). Fig. 3 also shows that this trend holds for Gr/(V_{0.02}Mo_{0.98}S₂+V_S), Gr/(V_{0.02}Mo_{0.98}S₂+V_{S-S}), Gr/(V_{0.02}Mo_{0.98}S₂+V_{2S}) (HST9, 10, 11), thus S mono and divacancies in the 2% doped TMDC do not affect the overall lack of magnetic moment in the HSTs. Moreover, $M_{tot} = 2 \mu_B$ of the stand-alone V_{0.04}Mo_{0.96}S₂ becomes $M_{tot} = 0.736 \mu_B$ for Gr/V_{0.04}Mo_{0.96}S₂. This reduction in the total magnetic moment is directly associated with charge transfer from Gr to V-doped MoS₂ layer regardless of point defect presence, as discussed below. Nevertheless, there are situations where the Gr layer enhances the FM properties of the standalone TMDC. Such is the case of a V-doped MoS₂ with a Mo monovacancy or a Mo+2S complex defect. The Gr monolayer enhances the M_{tot} by about 88% and 33% when compared to the isolated V_{0.02}Mo_{0.98}S₂+V_{Mo} or V_{0.02}Mo_{0.98}S₂+V_{Mo+2S}. Figs. 3b, c show that in all HSTs containing a pristine Gr monolayer, the magnetic properties are carried out by the TMDC monolayer, and Gr remains nonmagnetic.

The magnetic properties of the HSTs with a defective Gr layer are overall greatly enhanced compared with those of the standalone TMDC layer and the HST with the pristine Gr layer. We find that the total magnetic moment of Gr with C monovacancy is $1.271 \mu_B$. The FM state of (Gr+V_C) agrees with the well-known Lieb theorem that C monovacancy induces a magnetic moment on Gr while other defects do not.^{27,28} We further find that (Gr+V_C)/TMDC with the S point defects shows a prominent ferromagnetism with $M_{tot} > 1 \mu_B$ unlike the nonmagnetic TMDC monolayer or the weakly ferromagnetic Gr/TMDC system. This enhancement effect is even stronger for the (Gr+V_C)/(MoS₂+V_{Mo}) and (Gr+V_C)/(MoS₂+V_{Mo+2S}). The magnetic moments for (Gr+V_C)/V_{0.02}Mo_{0.98}S₂ and (Gr+V_C)/V_{0.04}Mo_{0.96}S₂ are 1.157 and 1.513 μ_B , respectively. It is also interesting to note



that the defective Gr has elevated M_{tot} for its HSTs formed with a doped TMDC with $(Gr+V_C)/(V_{0.02}Mo_{0.98}S_2+V_{Mo})$ and $(Gr+V_C)/(V_{0.02}Mo_{0.98}S_2+V_{Mo+2S})$ defects, for which Gr/TMDC showed weak ferromagnetism. It appears that in such cases, the magnetization is carried out primarily by the defective Gr layer (Fig. 3b, c). Introducing V dopants, however, enhances the magnetization of the TMDC layer itself, while Gr+ V_C remains ferromagnetic as well. Thus, these results show that the C vacancy plays a key role in the overall magnetic properties of the entire HST because it enhances the magnetization of the Gr layer itself. Such enhancement due to the ferromagnetism of the defective Gr layer is consistent with the enhanced magnetism found in other HSTs involving TMDC monolayers and ferromagnetic layers.^{15,29,30}

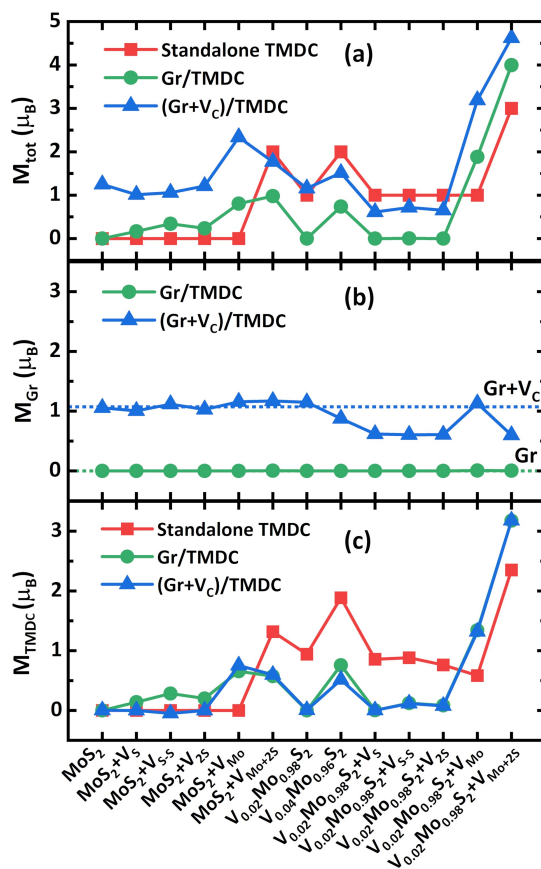


Figure 3: Magnetic moments of the: (a) entire HST M_{tot} (μ_B), (b) Gr layer M_{Gr} (μ_B), (c) TMDC layer M_{TMDC} (μ_B) as part of HSTs. The data is given as a function of the different TMDC used to construct each HST.



Further insight of the ferromagnetism of these systems can be gained by examining the electron spin density property. In Fig. 4, we show some representative cases by giving the electron spin density distribution with TMDC on top of the Gr layer. Gr/ $V_{0.02}Mo_{0.98}S_2$ is non-magnetic and no spin density appears between atoms in this system (Fig. 4a). The nearest Mo-site spins are antiferromagnetically coupled to the V-site spin, while the nearest S-site spins are ferromagnetically coupled to the V-site spin in $V_{0.04}Mo_{0.96}S_2$ monolayer. However, both the nearest Mo and S-site spins couple antiferromagnetically with the V-site spin in $V_{0.04}Mo_{0.96}S_2$ layer of Gr/ $V_{0.04}Mo_{0.96}S_2$ HST (Fig. 4b). Although the Gr/($V_{0.02}Mo_{0.98}S_2 + V_{S-S}$) HST has a total magnetic moment of zero, the antiferromagnetic orders appeared around the V atom ($0.807 \mu_B$) in the TMDC layer (Fig. 4c). In $V_{0.02}Mo_{0.98}S_2 + V_{Mo+2S}$ sheet of Gr/($V_{0.02}Mo_{0.98}S_2 + V_{Mo+2S}$) HST, the antiferromagnetic orders appeared on the nearest Mo and S atoms around V atom, while the ferromagnetic orders appeared on the nearest Mo and S atoms around vacancy. In this case, we can clearly see that the spin density is located not only on the atoms but also on the empty spaces (Fig. 4d). Spin density distributions are not found in the Gr sheets of these HSTs, which are consistent with the values shown in Fig. 3b. For defective Gr sheet of (Gr+ V_C)/TMDC HSTs, the C monovacancy produces two pentagons while the FM order is observed in one pentagon and the AFM order is observed in another pentagon (Fig. 4e-h). In (Gr+ V_C)/ $V_{0.02}Mo_{0.98}S_2$ HST, no spin density is observed in $V_{0.02}Mo_{0.98}S_2$ component (Fig. 4e). In (Gr+ V_C)/ $V_{0.04}Mo_{0.96}S_2$ HST, both V atoms have negative magnetic moments, but only one AFM order is observed for the nearest Mo and S atoms (Fig. 4f). Interestingly, spin density distributions of $V_{0.02}Mo_{0.98}S_2 + V_{S-S}$ or $V_{0.02}Mo_{0.98}S_2 + V_{Mo+2S}$ are almost unchanged in HSTs with the pristine or defective Gr sheets (Figs. 4g, h).

We also examined the magnetic moments of $V_{0.02}Mo_{0.98}S_2$ with various vacancies placed on Gr with C divacancies or SW defect and found that the magnetic phenomena in these systems are similar to those observed in pristine Gr. This is because the three systems pristine Gr, Gr+ V_{2C} and Gr+ V_{SW} are nonmagnetic.



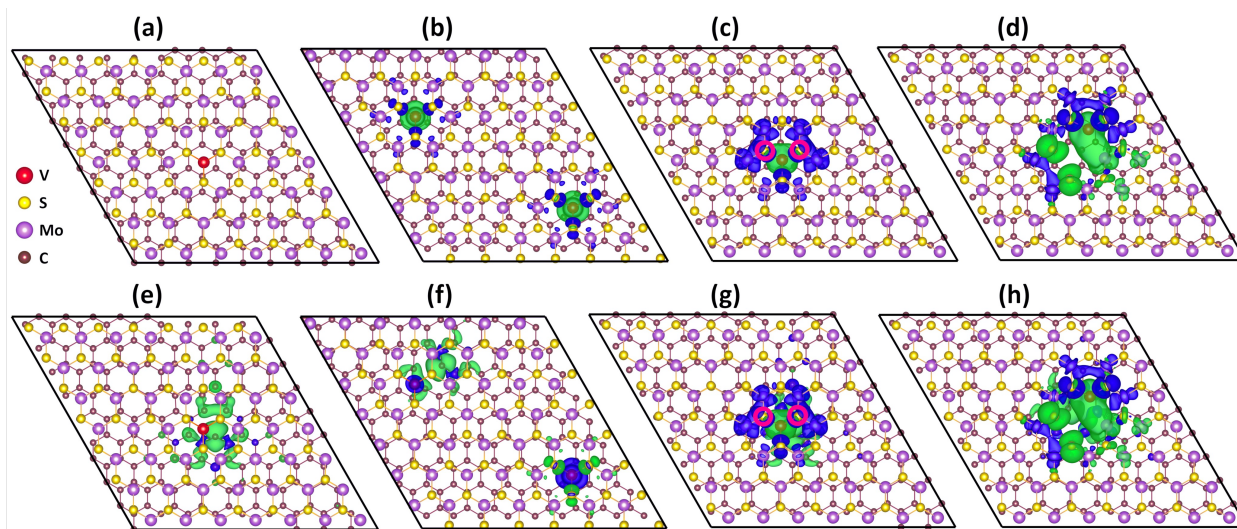


Figure 4: Electron spin densities of: (a) Gr/ $V_{0.02}Mo_{0.98}S_2$, (b) Gr/ $V_{0.04}Mo_{0.96}S_2$, (c) Gr/($V_{0.02}Mo_{0.98}S_2+V_{S-S}$), (d) Gr/($V_{0.02}Mo_{0.98}S_2+V_{Mo+2S}$), (e) (Gr+ V_C)/ $V_{0.02}Mo_{0.98}S_2$, (f) (Gr+ V_C)/ $V_{0.04}Mo_{0.96}S_2$, (g) (Gr+ V_C)/($V_{0.02}Mo_{0.98}S_2+V_{S-S}$) and (h) (Gr+ V_C)/($V_{0.02}Mo_{0.98}S_2+V_{Mo+2S}$) HSTs. Green and blue colors represent the spin-up and spin-down charges, respectively. The pink circles represent S vacancy positions. The isosurface value is $10^{-3} e/\text{\AA}^3$.

2.3 Electronic Structures Properties

We further discuss the electronic properties of the HSTs by analyzing their band structures (Figs. 5-6). For better clarity, the band structures for the individual layers in each HST are presented. Metallic behavior is observed for all cases except for the pristine Gr/ MoS_2 showing to be a semi-metal (Fig. 5a). In all cases, the well-known Dirac cones of an isolated Gr monolayer are maintained upon HST formation with the TMDC.

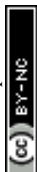
Fig. 5b shows that V doping is responsible for the electronic state of Gr/ $V_{0.02}Mo_{0.98}S_2$ HST becoming metallic. There is an upward shift of the electron states occupied in the valence band of the TMDC layer compared to that of the pristine HST, confirming the electron depletion from the Gr to the $V_{0.02}Mo_{0.98}S_2$ sheet. Increasing the concentration of V doping causes the electron states occupied in the valence band to continue to shift upward, resulting in an impurity state near the Fermi level (Fig. 5c). For Gr/ $V_{0.02}Mo_{0.98}S_2$ with vacancies, the defective states appear mainly in the gap region of the $V_{0.02}Mo_{0.98}S_2$ system



(Fig. 5d).

The band structures of the defective Gr in (Gr+V_C)/TMDC HSTs show that the bands for both spin carriers cross the Fermi energy (near the Γ point) (Fig. 6). Similarly to Gr, the band structures of Gr+V_C in these HSTs show upward shifts of the Dirac points. The position of the Dirac points above the Fermi level reflects the number of electrons transferred from the Gr+V_C to the TMDC monolayer. A notable difference between the band structures of Gr+V_C in these HSTs is the different locations of the σ bands around the energy range of -1 to -0.5 eV. The band structures of the TMDC components in (Gr+V_C)/TMDC HSTs are almost unchanged compared to those in Gr/TMDC HSTs.

Upon the introduction of the C monovacancy in Gr as part of each HST, one of linear π - π^* crossing bands breaks its degeneracy turning it into a quadratically dispersing one (Fig. 6). The spin-splitting gap between these bands depends on the V doping and vacancy concentrations in the TMDC layer. In particular, the introduction of V dopants at 2% concentration (Fig. 6b) increases the spin splitting gap while 4% concentration of V dopants (Fig. 6c) reduces the spin splitting gap when compared to the pristine TMDC (Fig. 6a). In the (Gr+V_C)/V_{0.02}Mo_{0.98}S₂ HST (Fig. 6b), the Fermi level crosses the spin-up π band but lies completely below the entire spin-down π band, which causes a slight increase in the defective Gr magnetism. On the other hand, in the (Gr+V_C)/V_{0.04}Mo_{0.96}S₂ HST (Fig. 6c), the Fermi level lies completely below both spin-up and -down π bands and leads to a small reduction in the defective Gr magnetism. Furthermore, when (Mo+2S) vacancies are present in the V dopants with 2% concentration (Fig. 6d), the splitting of π and π^* bands is similar to that in defect-free HST (Fig. 6b). However, the (Mo+2S) vacancies in TMDC layer reverses the spin polarizations of the π and π^* bands. This reversal reduces the magnetism in the defective Gr layer in (Gr+V_C)/(V_{0.02}Mo_{0.98}S₂+V_{Mo+2S}) HST compared to the corresponding defect-free (Gr+V_C)/V_{0.02}Mo_{0.98}S₂ HST.



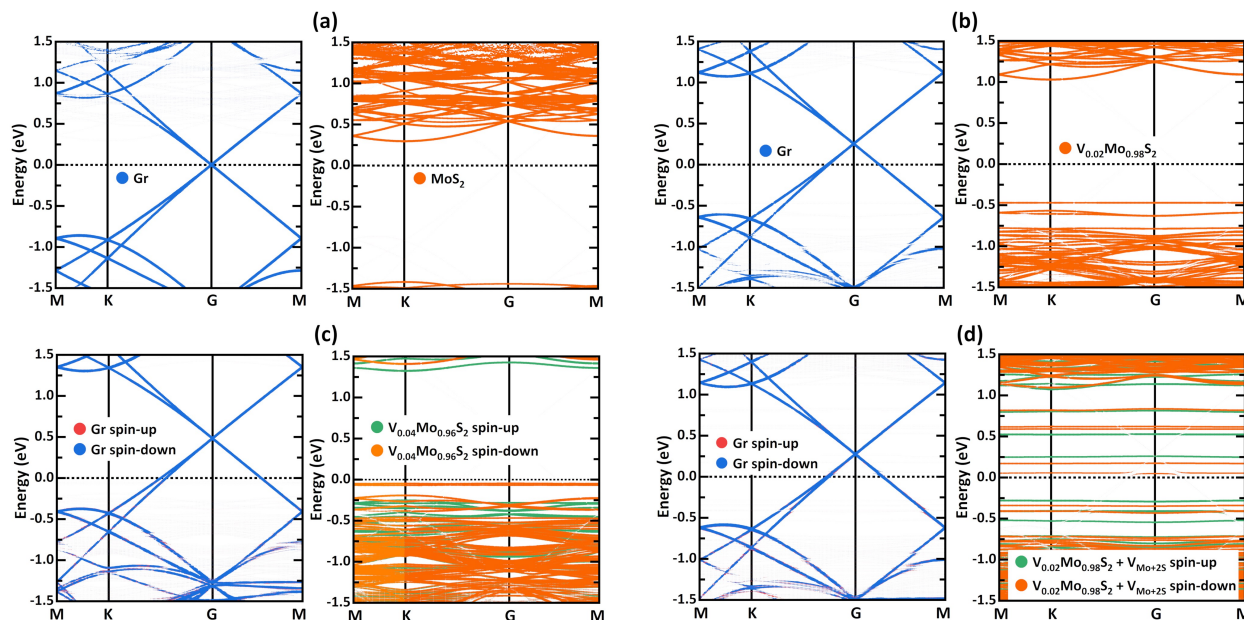


Figure 5: Band structures of (a) Gr/MoS₂, (b) Gr/V_{0.02}Mo_{0.98}S₂, (c) Gr/V_{0.04}Mo_{0.96}S₂ and (d) Gr/(V_{0.02}Mo_{0.98}S₂+V_{Mo+2S}) HSTs where the dotted lines represent the Fermi level.

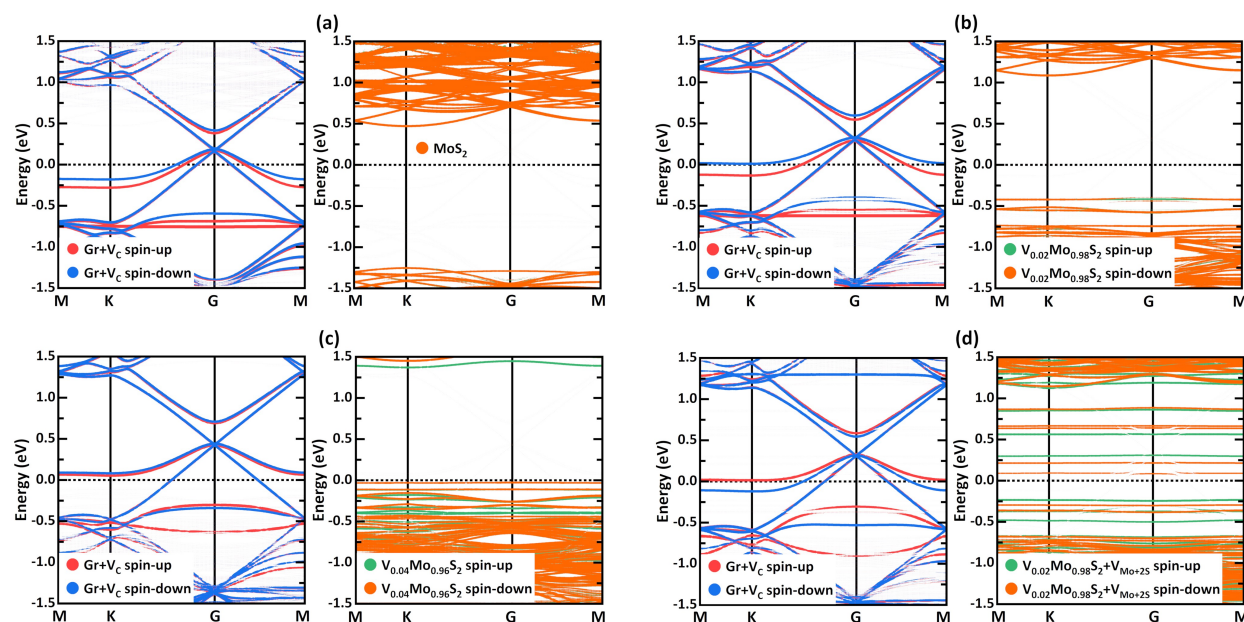


Figure 6: Band structures of (a) (Gr+V_C)/MoS₂, (b) (Gr+V_C)/V_{0.02}Mo_{0.98}S₂, (c) (Gr+V_C)/V_{0.04}Mo_{0.96}S₂ and (d) (Gr+V_C)/(V_{0.02}Mo_{0.98}S₂+V_{Mo+2S}) HSTs where the dotted lines represent the Fermi level.

The charge transfer in each HST is closely related to its electronic structure; thus, we



also calculate the 3D charge density differences in each case. The results are shown in Fig. 7. We find that generally electrons are transferred from Gr or (Gr+V_C) to the TMDC monolayer. No significant charge transfer is observed between Gr and MoS₂ (Fig. 7a), which is also found experimentally.³¹ Significant charge transfer is observed between the Gr and V_{0.02}Mo_{0.98}S₂ (Fig. 7b). The creation of vacancies or the increase in the doping concentration of V also significantly increases the charge transfer between the Gr and the TMDC layers (Figs. 7c, d). This is consistent with previous theoretical and experimental papers in other HSTs involving V-doped TMDCs (Fe/W_{0.967}V_{0.033}Se₂/Pt, Bi₂O₂Se/WS₂-V).^{29,32} The charge transfers between the defective Gr and TMDCs are comparatively higher than those observed between the pristine Gr and TMDCs (Figs. 7e-h). We can see that a significant portion of the charge density is localized on the C atoms near the defect sites, which results in a stronger interaction between the defective Gr and TMDC HSTs.

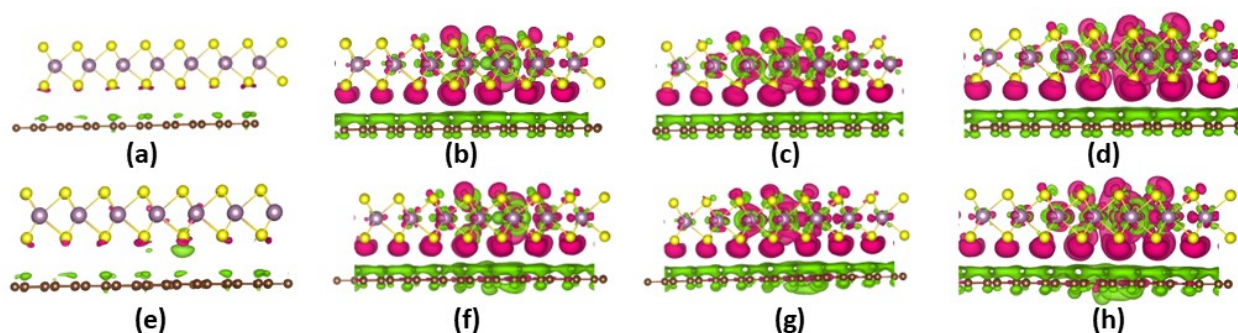


Figure 7: Charge density differences of (a) Gr/MoS₂, (b) Gr/V_{0.02}Mo_{0.98}S₂, (c) Gr/(V_{0.02}Mo_{0.98}S₂+V_{Mo+2S}) (d) Gr/V_{0.04}Mo_{0.96}S₂, (e) (Gr+V_C)/MoS₂, (f) (Gr+V_C)/V_{0.02}Mo_{0.98}S₂, (g) (Gr+V_C)/(V_{0.02}Mo_{0.98}S₂+V_{Mo+2S}) and (h) (Gr+V_C)/V_{0.04}Mo_{0.96}S₂ HSTs. The isosurface values are $3 \times 10^{-4} e/\text{\AA}^{-3}$. The pink isosurfaces represent the charge accumulation, the green isosurfaces represent the charge depletion.



2.4 Experimental observation of enhanced magnetization in V-doped MoS₂/Graphene heterostructures

To experimentally validate the DFT calculations of increased magnetization in the defective and doped MoS₂/Gr HSTs, we also report measurements of the V-doped MoS₂ monolayers and V-doped MoS₂/Gr HSTs alongside reference samples including pristine MoS₂ monolayers and MoS₂/Gr system. Details on the growth processes of these samples are provided in the Experimental Methods section. Magnetic measurements were carried out using a vibrating sample magnetometry (VSM) probe integrated into a physical property measurement system (PPMS) over a temperature range of 10–300 K. In all magnetic measurements, the magnetic field was applied parallel to the plane of the monolayer films. The results are given in Fig. 8(a-d). We observed that shown 2% Vanadium doping induces FM ordering at room temperature, resulting in enhanced saturation magnetization M_S in the V-doped MoS₂ (Fig. 8(a)) compared to the pristine MoS₂ monolayer (Fig. 8(d)). As expected, pristine MoS₂ monolayers grown on Si/SiO₂ substrates exhibit a weak FM signal, likely originating from various intrinsic vacancy defects.^{14,33} Our DFT calculations support this, showing that specific defect configurations (e.g. V_{Mo+2S} vacancies) dominantly induce FM ordering in the MoS₂ monolayer. Other studies have also shown that the MoS₂ net magnetic moment increases proportionally with the density of V_{Mo+2S} vacancies.³⁴ Experiments have indeed demonstrated the presence of S and/or Mo vacancies in CVD-grown MoS₂ and V-doped MoS₂ monolayers.^{14,26}



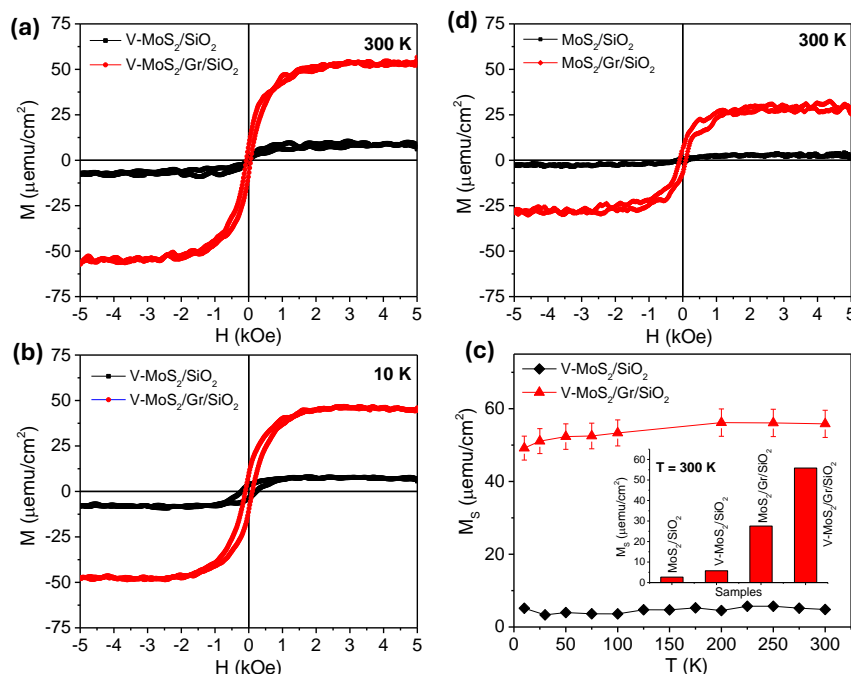


Figure 8: Magnetic hysteresis loops of the V-doped MoS₂ and V-doped MoS₂/Gr samples at (a) 300 K and (b) 10 K; (c) Temperature dependence of saturation magnetization for the V-doped MoS₂ and V-doped MoS₂/Gr samples; (d) Magnetic hysteresis loops taken at 300 K for the MoS₂ and MoS₂/Gr samples.

Notably, when the V-doped MoS₂ monolayer is stacked with Graphene, the M_S increases dramatically in the HST compared to the V-doped monolayer alone (Fig. 8(a,b)). At room temperature M_S increases from $\sim 5.67 \mu\text{emu}/\text{cm}^2$ in the doped TMDC to $\sim 55.83 \mu\text{emu}/\text{cm}^2$ in the HST. As shown in Fig. 8(c), this enhancement persists across the full temperature range of 10 - 300 K. Moreover, the M_S of the V-doped MoS₂/Gr system (Fig. 8(a)) is nearly doubled of the undoped MoS₂/Gr (Fig. 8(d)). Compared to the isolated MoS₂ or V-doped MoS₂ monolayers, the increase in magnetization upon interfacing with graphene in our HSTs is also consistent with reports on TMDC/Gr systems.^{15,16} For example, Cai et al¹⁶ suggest that covalent interactions at the MoS₂ Moiré superlattice/graphene oxide interface, such as the formation of Mo-S-C bonds, lead to spin polarization of Mo 4d electrons near the Fermi level, thereby inducing high-temperature FM ordering in the HST. However, such interfacial effects alone cannot explain the substantial M_S enhancement observed in our



MoS₂/Gr systems (Fig. 8(a,d)). The study¹⁵ has demonstrated that vacancy defects play a critical role in inducing ferromagnetic ordering in the MoS₂ monolayer as part of Mn-doped MoS₂/Gr systems.

A comparison between Fig. 8(a,d) suggests that the Graphene interfacing effect contributes more to the overall magnetization than V-doping alone. The combined effect of V-doping and MoS₂/Gr interfacing results in the highest observed M_S in the V-doped MoS₂/Gr HST (see the inset of Fig. 8(c)), surpassing both the V-doped MoS₂ monolayer and the MoS₂/Gr HST. These experimental observations are fully supported by our DFT simulations, which also predict that the presence of (C, S, Mo) vacancies in both Graphene and TMDC layers can enhance the overall magnetization, particularly when these defects are close and located near the interface. Electron transfer from MoS₂ to Graphene further strengthens the FM coupling between V magnetic ions via p-d orbital hybridization (Fig. 7(b)), contributing to the observed magnetization enhancement. Compared to the undoped HST, the charge transfer effect appears significantly stronger in the V-doped MoS₂/Gr system, especially in those with V_{Mo} and V_{Mo+2S} vacancies. Our combined theoretical and experimental findings not only validate the magnetization enhancement predicted for Mn-doped MoS₂/Gr heterostructures,¹⁵ but also provide new insights into the underlying physical mechanisms driving FM ordering in the 2D TMDC/Gr systems adding new functionalities to 2D van der Waals heterostructure-based nanodevices.^{35,36}

3 Conclusions

The present study reports on the geometric, electronic and magnetic properties of V-doped MoS₂/Gr HSTs with relatively low V doping. All considered HSTs are metallic in nature, except the pristine Gr/MoS₂ showing to be a semi-metal, with charge transfer from the Gr layer to the TMDC layer. This type of charge transfer is enhanced in the defective HSTs with a significant portion of the charge density localized near the defect sites.



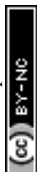
We further find that Gr/MoS₂ is nonmagnetic when doped with 2% V and becomes ferromagnetic with a total magnetic moment of 3 μ_B /cell as the V doping concentration increases. The V-doped MoS₂/Gr HST with 4% V doping experiences stronger charge transfer as well as an upshift of the Dirac point. The effects of various defects, such as C monovacancy and Mo, S vacancies on the structural, electronic, and magnetic properties of V-doped MoS₂/Gr HSTs with 2% V doping are also studied. The overall geometry and stability of HSTs change insignificantly in the presence of defects. However, the defects in both Gr and V-doped MoS₂ control the magnetic properties of the resulting HSTs. Pristine Gr remains nonmagnetic in all studied HSTs, while defective Gr displays strong magnetic properties. On the other hand, S mono and divacancies have secondary effects on the overall magnetization in the Gr/TMDC and (Gr+V_C)/TMDC HSTs, respectively. In contrast, the Mo monovacancy and (Mo+2S) complex defect in the 2% doped TMDC noticeably affect the overall magnetization in the Gr/TMDC and (Gr+V_C)/TMDC HSTs, respectively.

This study sheds light on the complex magnetism in sharp interfaced HSTs composed of Graphene and a TMDC monolayer when doping and defects are taken into account. Tuning ferromagnetism in 2D systems by varying doping concentration and defect engineering is an attractive pathway for targeted applications in spintronics and other areas.

4 Methods

4.1 Computational methods

The first-principles calculations are performed in the Vienna ab-initio simulation package (VASP)³⁷ based on density functional theory (DFT)³⁸ and the projector augmented wave (PAW) method.³⁹ The PAW potentials describe the core states of C, Mo, S and V by the electronic configurations of [He]2s²2p², [Ar]4s²3d¹⁰, [Ne]3s²3p⁴ and [Ar]3d³4s², respectively. The Perdew-Burke-Ernzerhof (PBE) parameterization of the generalized gradient approximation (GGA) is employed to describe the exchange–correlation function.⁴⁰ The structures



have been optimized using the conjugate gradient method with the forces calculated using the Hellman-Feynman theorem. The convergence criteria for the total energy and residual force on each atom are set to 10^{-5} eV and 10^{-2} eV/Å, respectively. To isolate the interaction between the HST and its periodic images, a vacuum layer with a thickness of 15 Å is inserted along the direction perpendicular to the layers. In addition, the DFT-D3(BJ) approach⁴¹ is used to correct the vdW interaction in the HSTs. Considering the strong correlation effect of the V-3d electrons, a simplified DFT+U approach⁴² is employed with $U_{eff} = 3$ eV.²⁹ The plane-wave energy cutoff is set to 500 eV, and a Γ -centered k meshes of $2 \times 2 \times 1$ is adopted to sample the first Brillouin zone for geometry optimization. The total energies and electronic structures are calculated with the optimized structures on a $9 \times 9 \times 1$ Monkhorst-Pack k-grid. The planar-averaged differential charge density offers a quantitative base for analyzing interfacial charge redistribution, which is defined as $\Delta\rho = \rho_{L1/L2} - \rho_{L1} - \rho_{L2}$ where $\rho_{L1/L2}$, ρ_{L1} and ρ_{L2} are the planar-averaged charge density of the HST and the isolated monolayers constituted the HST, respectively.

4.2 Experimental methods

Pristine MoS₂ and V-doped MoS₂ monolayers were synthesized via chemical vapor deposition (CVD) and subsequently wet-transferred onto a CVD-grown graphene monolayer supported on a SiO₂/Si substrate. A Vanadium doping concentration of 2 at% was selected for this study, consistent with our previous work.¹⁴ The Vanadium doping level was controlled by adjusting the V:Mo ratio in the precursor mixture. Additional factors such as source placement, temperature gradient, carrier gas flow rate, and substrate positioning were also carefully optimized for the control of the doping concentration. The Graphene monolayer was prepared through the thermal decomposition of a carbon-rich precursor, leading to the deposition of carbon atoms in a honeycomb lattice atop a copper film, which served as the catalytic substrate. After growth, the graphene layer was coated with polymethyl methacrylate (PMMA), and the underlying copper was etched away prior to transfer onto the SiO₂/Si



substrate. The MoS₂/Gr and V-doped MoS₂/Gr HSTs were annealed at 300°C for 10 hours to remove PMMA residues introduced during the transfer process. Post-annealing, the inter-layer spacing between the V-doped MoS₂ and Graphene was measured to be approximately 1.5 nm. For comparison, pristine and V-doped MoS₂ monolayers were also annealed under the same conditions.

The structural properties of both pristine and V-doped TMDC monolayers, as well as their corresponding TMDC/Graphene HSTs, were characterized using scanning transmission electron microscopy (STEM) and atomic force microscopy (AFM). The optical responses were examined via Raman and photoluminescence (PL) spectroscopy. Magnetic properties were measured using a vibrating sample magnetometry (VSM) probe integrated into a physical property measurement system (PPMS), under magnetic fields up to 9 T and across a broad temperature range from 2 K to 400 K.

Acknowledgement

D.T-X.D. acknowledges support from Presidential Fellowship sponsored by University of South Florida. L.M.W. acknowledges financial support from the US Department of Energy under Grant No.DE-FG02-06ER46297. Computational resources are provided by USF Research Computing. M.H.P acknowledges support from the US Department of Energy, Office of Basic Energy Sciences, Division of Materials Science and Engineering under Grant No. DE-FG02-07ER46438 (magnetic measurements).

Author information

Corresponding Author

- Manh-Huong Phan - Department of Physics, University of South Florida, Tampa, Florida 33620, United States; orcid.org/0000-0002-6270-8990 Email: phanm@usf.edu.



- Lilia M. Woods - Department of Physics, University of South Florida, Tampa, Florida 33620, United States; orcid.org/0000-0002-9872-1847; Email: lmwoods@usf.edu.

Authors

- Diem Thi-Xuan Dang - Department of Physics, University of South Florida, Tampa, Florida 33620, United States; orcid.org/0000-0001-7136-4125.
- Yen Thi-Hai Pham - Department of Physics, University of South Florida, Tampa, Florida 33620, United States; Current address: Department of Physics and Astronomy, George Mason University, Fairfax, Virginia 22030, USA.
- Da Zhou - Department of Physics & Center for 2-Dimensional and Layered Materials, The Pennsylvania State University, University Park, Pennsylvania 16802, USA.
- Dai-Nam Le - Department of Physics, University of South Florida, Tampa, Florida 33620, United States; orcid.org/0000-0003-0756-8742.
- Mauricio Terrones - Department of Physics & Center for 2- Dimensional and Layered Materials, The Pennsylvania State University, University Park, Pennsylvania 16802, USA.

Conflicts of Interest

There are no conflicts to declare.

Data Availability

All data that support the findings of this study have been included in this publication.



References

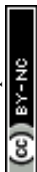
- (1) Luo, Y. K.; Xu, J.; Zhu, T.; Wu, G.; McCormick, E. J.; Zhan, W.; Neupane, M. R.; Kawakami, R. K. Opto-valleytronic spin injection in monolayer MoS₂/few-layer graphene hybrid spin valves. *Nano Letters* **2017**, *17*, 3877–3883, DOI: 10.1021/acs.nanolett.7b01393.
- (2) Avsar, A.; Unuchek, D.; Liu, J.; Sanchez, O. L.; Watanabe, K.; Taniguchi, T.; Ozyilmaz, B.; Kis, A. Optospintronics in graphene via proximity coupling. *ACS Nano* **2017**, *11*, 11678–11686, DOI: 10.1021/acsnano.7b06800.
- (3) Ghiasi, T. S.; Kaverzin, A. A.; Blah, P. J.; Van Wees, B. J. Charge-to-spin conversion by the Rashba–Edelstein effect in two-dimensional van der Waals heterostructures up to room temperature. *Nano Letters* **2019**, *19*, 5959–5966, DOI: 10.1021/acs.nanolett.9b01611.
- (4) Benitez, L. A.; Savero Torres, W.; Sierra, J. F.; Timmermans, M.; Garcia, J. H.; Roche, S.; Costache, M. V.; Valenzuela, S. O. Tunable room-temperature spin galvanic and spin Hall effects in van der Waals heterostructures. *Nature Materials* **2020**, *19*, 170–175, DOI: 10.1038/s41563-019-0575-1.
- (5) Zhang, F.; Zheng, B.; Sebastian, A.; Olson, D. H.; Liu, M.; Fujisawa, K.; Pham, Y. T. H.; Jimenez, V. O.; Kalappattil, V.; Miao, L.; others Monolayer vanadium-doped tungsten disulfide: a room-temperature dilute magnetic semiconductor. *Advanced Science* **2020**, *7*, 2001174, DOI: 10.1002/advs.202001174.
- (6) Coelho, P. M. Magnetic doping in transition metal dichalcogenides. *Journal of Physics: Condensed Matter* **2024**, *36*, 203001, DOI: 10.1088/1361-648X/ad271b.
- (7) Pham, Y. T. H.; Liu, M.; Jimenez, V. O.; Yu, Z.; Kalappattil, V.; Zhang, F.; Wang, K.; Williams, T.; Terrones, M.; Phan, M.-H. Tunable ferromagnetism and thermally in-



- duced spin flip in Vanadium-doped tungsten diselenide monolayers at room temperature. *Advanced Materials* **2020**, *32*, 2003607, DOI: 10.1002/adma.202003607.
- (8) Ortiz Jimenez, V.; Pham, Y. T. H.; Liu, M.; Zhang, F.; Yu, Z.; Kalappattil, V.; Mucharla, B.; Eggers, T.; Duong, D. L.; Terrones, M.; others Light-controlled room temperature ferromagnetism in vanadium-doped tungsten disulfide semiconducting monolayers. *Advanced Electronic Materials* **2021**, *7*, 2100030, DOI: 10.1002/aelm.202100030.
- (9) Yun, S. J.; Duong, D. L.; Ha, D. M.; Singh, K.; Phan, T. L.; Choi, W.; Kim, Y.-M.; Lee, Y. H. Ferromagnetic order at room temperature in monolayer WSe₂ semiconductor via vanadium dopant. *Advanced Science* **2020**, *7*, 1903076, DOI: <https://doi.org/10.1002/advs.201903076>.
- (10) Nguyen, L.-A. T.; Jiang, J.; Nguyen, T. D.; Kim, P.; Joo, M.-K.; Duong, D. L.; Lee, Y. H. Electrically tunable magnetic fluctuations in multilayered vanadium-doped tungsten diselenide. *Nature Electronics* **2023**, *6*, 582–589, DOI: <https://doi.org/10.1038/s41928-023-01002-1>.
- (11) Zhang, J.; Zhu, Y.; Tebyetekerwa, M.; Li, D.; Liu, D.; Lei, W.; Wang, L.; Zhang, Y.; Lu, Y. Vanadium-doped monolayer MoS₂ with tunable optical properties for field-effect transistors. *ACS Applied Nano Materials* **2020**, *4*, 769–777, DOI: 10.1021/acsanm.0c03083.
- (12) Sahoo, K. R.; Panda, J. J.; Bawari, S.; Sharma, R.; Maity, D.; Lal, A.; Arenal, R.; Rajalaksmi, G.; Narayanan, T. N. Enhanced room-temperature spin-valley coupling in V-doped MoS₂. *Physical Review Materials* **2022**, *6*, 085202, DOI: 10.1103/PhysRevMaterials.6.085202.
- (13) Maity, D.; Sharma, R.; Sahoo, K. R.; Lal, A.; Arenal, R.; Narayanan, T. N. On the existence of photoluminescence and room-temperature spin polarization in ambipolar V doped MoS₂ monolayers. *arXiv preprint arXiv:2204.05887* **2022**,



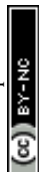
- (14) Zhou, D.; Pham, Y. T. H.; Dang, D. T.-X.; Sanchez, D.; Oberoi, A.; Wang, K.; Fest, A.; Sredenschek, A.; Liu, M.; Terrones, H.; Das, S.; Le, D.-N.; Woods, L. M.; Phan, M.-H.; Terrones, M. Vanadium-doped molybdenum disulfide monolayers with tunable electronic and magnetic properties: do vanadium-vacancy pairs matter? *arXiv preprint arXiv:2401.16806* **2024**,
- (15) Tan, Q.; Wang, Q.; Liu, Y.; Liu, C.; Feng, X.; Yu, D. Enhanced magnetic properties and tunable Dirac point of graphene/Mn-doped monolayer MoS₂ heterostructures. *Journal of Physics: Condensed Matter* **2018**, *30*, 305304, DOI: 10.1088/1361-648X/aacca2.
- (16) Cai, L.; Duan, H.; Liu, Q.; Wang, C.; Tan, H.; Hu, W.; Hu, F.; Sun, Z.; Yan, W. Ultrahigh-temperature ferromagnetism in MoS₂ Moiré superlattice/graphene hybrid heterostructures. *Nano Research* **2021**, *14*, 4182–4187, DOI: <https://doi.org/10.1007/s12274-021-3360-9>.
- (17) Nakhmedov, E.; Nadimi, E.; Vedaiei, S.; Alekperov, O.; Tatardar, F.; Najafov, A.; Abbasov, I.; Saletsky, A. Vacancy mediated magnetization and healing of a graphene monolayer. *Physical Review B* **2019**, *99*, 125125, DOI: 10.1103/PhysRevB.99.125125.
- (18) Tiwari, S. K.; Pandey, S. K.; Pandey, R.; Wang, N.; Bystrzejewski, M.; Mishra, Y. K.; Zhu, Y. Stone–wales defect in graphene. *Small* **2023**, *19*, 2303340, DOI: 10.1002/sml.202303340.
- (19) Lin, Z.; Carvalho, B. R.; Kahn, E.; Lv, R.; Rao, R.; Terrones, H.; Pimenta, M. A.; Terrones, M. Defect engineering of two-dimensional transition metal dichalcogenides. *2D Materials* **2016**, *3*, 022002, DOI: 10.1088/2053-1583/3/2/022002.
- (20) Han, X.; Niu, M.; Luo, Y.; Li, R.; Dan, J.; Hong, Y.; Wu, X.; Trukhanov, A. V.; Ji, W.; Wang, Y.; others Atomically engineering metal vacancies in monolayer transition metal dichalcogenides. *Nature Synthesis* **2024**, *3*, 586–594, DOI: 10.1038/s44160-024-00501-z.



- (21) Khan, M.; Erementchouk, M.; Hendrickson, J.; Leuenberger, M. N. Electronic and optical properties of vacancy defects in single-layer transition metal dichalcogenides. *Physical Review B* **2017**, *95*, 245435, DOI: 10.1103/PhysRevB.95.245435.
- (22) Koós, A. A.; Vancsó, P.; Szendrő, M.; Dobrik, G.; Antognini Silva, D.; Popov, Z. I.; Sorokin, P. B.; Henrard, L.; Hwang, C.; Biró, L. P.; others Influence of native defects on the electronic and magnetic properties of CVD grown MoSe₂ single layers. *The Journal of Physical Chemistry C* **2019**, *123*, 24855–24864, DOI: 10.1021/acs.jpcc.9b05921.
- (23) Yun, W. S.; Lee, J. D. Strain-induced magnetism in single-layer MoS₂: origin and manipulation. *The Journal of Physical Chemistry C* **2015**, *119*, 2822–2827, DOI: 10.1021/jp510308a.
- (24) Dang, D. T.-X.; Le, D.-N.; Woods, L. M. Dissecting van der Waals interactions with Density Functional Theory–Wannier-basis approach. *Computer Physics Communications* **2025**, 109525, DOI: 10.1016/j.cpc.2025.109525.
- (25) Wang, Y.; Li, S.; Yi, J. Electronic and magnetic properties of Co doped MoS₂ monolayer. *Scientific Reports* **2016**, *6*, 24153, DOI: 10.1038/srep24153.
- (26) Hu, W.; Tan, H.; Duan, H.; Li, G.; Li, N.; Ji, Q.; Lu, Y.; Wang, Y.; Sun, Z.; Hu, F.; Wang, C.; Yan, W. Synergetic effect of substitutional dopants and sulfur vacancy in modulating the ferromagnetism of MoS₂ nanosheets. *ACS Applied Materials Interfaces* **2019**, *11*, 31155–31161, DOI: <https://doi.org/10.1021/acsami.9b09165>.
- (27) Lieb, E. H. Two theorems on the Hubbard model. *Physical Review Letters* **1989**, *62*, 1201, DOI: 10.1103/PhysRevLett.62.1201.
- (28) Yazyev, O. V.; Helm, L. Defect-induced magnetism in graphene. *Physical Review B—Condensed Matter and Materials Physics* **2007**, *75*, 125408, DOI: 10.1103/PhysRevB.75.125408.



- (29) Thi-Xuan Dang, D.; Barik, R. K.; Phan, M.-H.; Woods, L. M. Enhanced magnetism in heterostructures with transition-metal dichalcogenide monolayers. *The Journal of Physical Chemistry Letters* **2022**, *13*, 8879–8887, DOI: 10.1021/acs.jpcllett.2c01925.
- (30) Hung, C.-M. et al. Enhanced magnetism and anomalous Hall transport through two-dimensional tungsten disulfide interfaces. *Nanomaterials* **2023**, *13*, DOI: 10.3390/nano13040771.
- (31) Pierucci, D.; Henck, H.; Avila, J.; Balan, A.; Naylor, C. H.; Patriarche, G.; Dappe, Y. J.; Silly, M. G.; Sirotti, F.; Johnson, A. T. C.; Asensio, M. C.; Ouerghi, A. Band alignment and minigaps in monolayer MoS₂-Graphene van der Waals heterostructures. *Nano Letters* **2016**, *16*, 4054–4061, DOI: 10.1021/acs.nanolett.6b00609.
- (32) Chitara, B.; Dimitrov, E.; Liu, M.; Seling, T. R.; Kolli, B. S.; Zhou, D.; Yu, Z.; Shringi, A. K.; Terrones, M.; Yan, F. Charge transfer modulation in Vanadium-doped WS₂/Bi₂O₂Se heterostructures. *Small* **2023**, *19*, 2302289, DOI: 10.1002/smll.202302289.
- (33) Cai, L.; He, J.; Liu, Q.; Yao, T.; Chen, L.; Yan, W.; Hu, F.; Jiang, Y.; Zhao, Y.; Hu, T.; Sun, Z.; Wei, S. Vacancy-induced ferromagnetism of MoS₂ nanosheets. *J. Am. Chem. Soc.* **2015**, *137*, 2622–2627, DOI: <https://doi.org/10.1021/ja5120908>.
- (34) Anbalagan, A. k. et al. Gamma-ray irradiation induced ultrahigh room-temperature ferromagnetism in MoS₂ sputtered few-layered thin films. *ACS Nano* **2023**, *17*, 6555–6564, DOI: <https://doi.org/10.1021/acsnano.2c11955>.
- (35) Safeer, C. K.; Ingla-Aynés, J.; Herling, F.; Garcia, J. H.; Vila, M.; Ontoso, N.; Calvo, M. R.; Roche, S.; Hueso, L. E.; Casanova, F. Room-temperature spin hall effect in graphene/MoS₂ van der waals heterostructures. *Nano Letters* **2019**, *19*, 1074–1082, DOI: <https://doi.org/10.1021/acs.nanolett.8b04368>.



- (36) Yu, L.; Lee, Y.-H.; Ling, X.; Santos, E. J. G.; Shin, Y. C.; Lin, Y.; Dubey, M.; Kaxiras, E.; Kong, J.; Wang, H.; Palacios, T. Graphene/MoS₂ hybrid technology for large-scale two-dimensional electronics. *Nano Letters* **2014**, *14*, 3055–3063, DOI: <https://doi.org/10.1021/nl404795z>.
- (37) Kresse, G.; Furthmüller, J. Efficient iterative schemes for ab initio total-energy calculations using a plane-wave basis set. *Physical Review B* **1996**, *54*, 11169, DOI: 10.1103/PhysRevB.54.11169.
- (38) Hohenberg, P.; Kohn, W. Inhomogeneous electron gas. *Physical Review* **1964**, *136*, B864, DOI: 10.1103/PhysRev.136.B864.
- (39) Kresse, G.; Joubert, D. From ultrasoft pseudopotentials to the projector augmented-wave method. *Physical Review B* **1999**, *59*, 1758, DOI: 10.1103/PhysRevB.59.1758.
- (40) Perdew, J. P.; Burke, K.; Ernzerhof, M. Generalized gradient approximation made simple. *Physical Review Letters* **1996**, *77*, 3865, DOI: 10.1103/PhysRevLett.77.3865.
- (41) Grimme, S.; Ehrlich, S.; Goerigk, L. Effect of the damping function in dispersion corrected density functional theory. *Journal of Computational Chemistry* **2011**, *32*, 1456–1465, DOI: 10.1002/jcc.21759.
- (42) Dudarev, S. L.; Botton, G. A.; Savrasov, S. Y.; Humphreys, C.; Sutton, A. P. Electron-energy-loss spectra and the structural stability of nickel oxide: An LSDA+ U study. *Physical Review B* **1998**, *57*, 1505, DOI: 10.1103/PhysRevB.57.1505.



Data Availability

All data that support the findings of this study have been included in this publication.

